A wearable acoustofluidic patch for rapid reversal of opioid overdose

Yantao Xing,[1,#] Yang Yang,[1,#] Xiang Li,[1,#] Hongwei Cai, [1] Zhuhao Wu,[1] Zheng Ao,[1] Chunhui Tian,[1] Vivian Niu,[1] Jack Crystal,[1] Gergő Szanda,[2] Taylor J Woodward,[2] Heather B. Bradshaw,[2] Han-Ting Chen,[2] Junhua Xu,[1,*] Ken Mackie,[2,*] and Feng Guo,[1,*]

1. Department of Intelligent Systems Engineering, Indiana University, Bloomington, IN 47405, United States
2. Gill Institute for Neuroscience, and Department of Psychological and Brain Sciences, Indiana University, Bloomington, IN 47405, United States

[#] Contributed equally to this work

[*] Corresponding email addresses:
xujh0709@gmail.com (J.X.), kmackie@iu.edu (K.M.), or fengguo@iu.edu (F.G.)

List of Contents

Supplementary Notes

AI algorithms for detecting opioid overdose

```
# Pseudocode: CNN-based Respiratory Signal Classification and Automated
Rescue

FUNCTION PreprocessData(raw_signal):
    # Preprocess the raw respiratory signal and convert it into the
required model input format
    processed_signal = Resize(raw_signal, (150, 1))
    RETURN processed_signal

FUNCTION ClassifyState(respiratory_signal):
    # Process the signal
    processed_signal = PreprocessData(respiratory_signal)

    # Perform prediction using the CNN model
    prediction = CNN_Model.Predict(processed_signal)

    # Determine whether the subject is overdosed
    IF prediction = 1 THEN
        RETURN "Overdosed"
    ELSE
        RETURN "Healthy"

FUNCTION TriggerRescue():
    # Execute rescue actions

    # 1. Send BLE command to activate the acoustic patch for drug delivery
    SEND_BLE_Command("wearable_device", "activate_patch")

    # 2. Dial the emergency contact via the cellular network
    Dial_EmergencyContact("pre-set_contact")

FUNCTION MonitorRespiratoryData():
    # Real-time monitoring of respiratory data
    WHILE True DO
        # Acquire real-time respiratory data
        raw_signal = AcquireSignal()

        # Perform classification
        state = ClassifyState(raw_signal)

        # Trigger rescue if an overdose is detected
        IF state == "Overdosed" THEN
            PRINT "Overdose detected! Initiating rescue operation..."
            TriggerRescue()
        ELSE
            PRINT "Status: Healthy"

# Start real-time monitoring
MonitorRespiratoryData()
```

Evaluation and metric for AI algorithms

Metrics for binary classification: confusion matrix, accuracy, precision-recall, and F1 score. The confusion matrix, also known as the error matrix, is a table used to visualize the accuracy between actual and predicted classes. For binary classification tasks, the confusion matrix is composed of positive and negative classes. When the model correctly predicts the positive class, it is defined as a True Positive (TP). Similarly, when the model correctly predicts the negative class, it is defined as a True Negative (TN). If the model incorrectly predicts the positive class, it is classified as a False Positive (FP), and if it incorrectly predicts the negative class, it is classified as a False Negative (FN). Precision is a measure of the relevance of the results, while recall evaluates how many of the truly relevant results are returned. They are defined as follows:

$$Precision = \frac{TP}{TP + FP}$$

$$Recall = \frac{TP}{TP + FN}$$

Accuracy represents the proportion of correct predictions out of all predictions made and is defined as:

$$Accuracy = \frac{TP + TN}{TP + FP + TN + FN}$$

F1 score is the harmonic mean of precision and recall:

$$F1 = 2 * \frac{Precision * Recall}{Precision + Recall}$$

Implementation of automated system and emergency report

Upon fentanyl administration, the wearable device initiates a respiration analysis process upon receiving a designated command and begins transmitting real-time data to the paired mobile device. If opioid-induced respiratory depression is detected, the mobile app first issues an alert before executing an automated rescue protocol. It transmits a command via Bluetooth Low Energy (BLE) to activate the patch, ensuring timely drug delivery. Simultaneously, the app uses the cellular network to relay an emergency call. In animal experiments, due to Federal Communications Commission regulations on non-emergency 9-1-1 calls, the system dialed a pre-designated emergency contact within the app rather than 9-1-1. In the case of mice, a python script replaced the mobile application for device control and data collection.

Dermal tolerance assessment

Dermal tolerance was evaluated by semi-quantitative scoring of erythema and edema at the indicated time points using a blinded assessment protocol. Both parameters were graded on a 0–4 scale adapted from standard dermal irritation scoring criteria. Detailed scoring criteria are provided below.

Erythema (redness):

Score	Description
0	No visible erythema
1	Very slight erythema (barely perceptible)
2	Well-defined erythema
3	Moderate to severe erythema
4	Severe erythema (deep redness and/or slight eschar formation)

Edema (swelling):

Score	Description
0	No edema
1	Very slight edema (barely perceptible)
2	Slight edema with clearly defined margins
3	Moderate edema with visible elevation (~1 mm)
4	Severe edema with marked swelling (>1 mm and/or extending beyond application area)

Histological and immunohistochemical evaluation of skin

Mouse skin tissues were collected 24 h after repeated microneedle application. Tissue sections were subjected to hematoxylin and eosin (H&E) staining and immunohistochemical staining using a rabbit monoclonal anti-CD31 antibody (Abcam, cat. no. ab182981, clone EPR17259; 1:1,000) and a rabbit monoclonal anti-F4/80 antibody (Cell Signaling Technology, cat. no. 70076, clone D2S9R; 1:500). A goat anti-rabbit IgG H&L antibody conjugated to horseradish peroxidase (HRP; Abcam, cat. no. ab205718; 1:2,000) was used as the secondary antibody. H&E and immunohistochemical staining were used to evaluate skin tissue architecture, vascular structures, and local macrophage presence following microneedle application.

Supplementary Figures

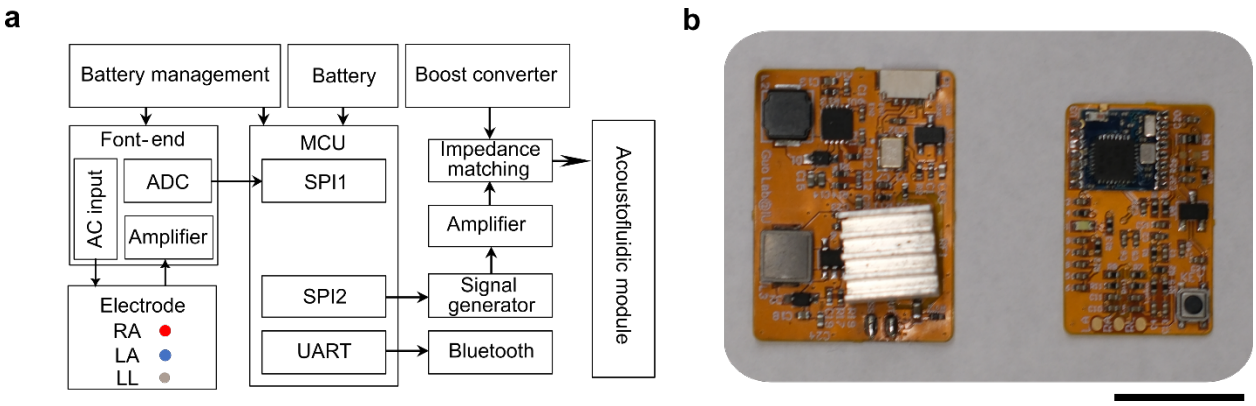

Supplementary Fig. 1 Design and prototype of electronic circuits for controlling patch systems. (**a**) Schematic diagram of electronic circuit design. The front-end components such as the electrodes (RA, LA, LL) are designed to collect signals and pass them through the analogue-to-digital converter (ADC) and amplifier. The microcontroller unit (MCU) is used to manage data transmission via serial peripheral interface 1 (SPI1) and SPI2, UART, and Bluetooth. The battery management unit can supply power, while the boost converter ensures stable voltage regulation. The impedance matching and signal generation modules are used to amplify and optimize signals before sending them to the acoustofluidic module. (**b**) Prototype of the circuits on a flexible printed circuit board (FPCB). Scale bar, 1 cm.

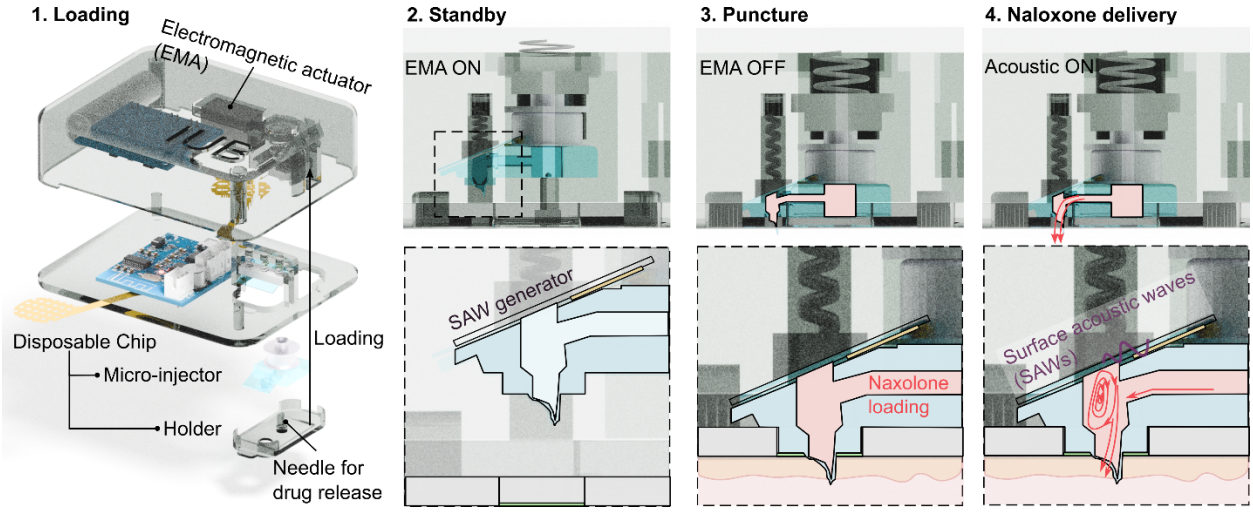

Supplementary Fig. 2 Workflow of acoustofluidic patch-mediated naloxone delivery. The structure of the acoustofluidic patch is illustrated on the left, comprising a device housing and a disposable chip. The workflow of acoustofluidic patch-mediated naloxone delivery is described as the following steps: (1) Loading: The chip, including micro-injector and drug capsule, is pressed into the device housing and sealed using the holder; (2) Standby: The SAW generator is aligned and bonded to the micro-injector through pressure; (3) Puncture: Upon receiving the puncture command, the EMA deactivates, allowing the micro-injector to be ejected downward by spring force, penetrating the skin. Simultaneously, the needle on the holder pierces the capsule, initiating drug release; and (4) Naloxone delivery: Following the delivery command, programmable acoustic actuation drives the fluid, enabling controlled and precise drug delivery.

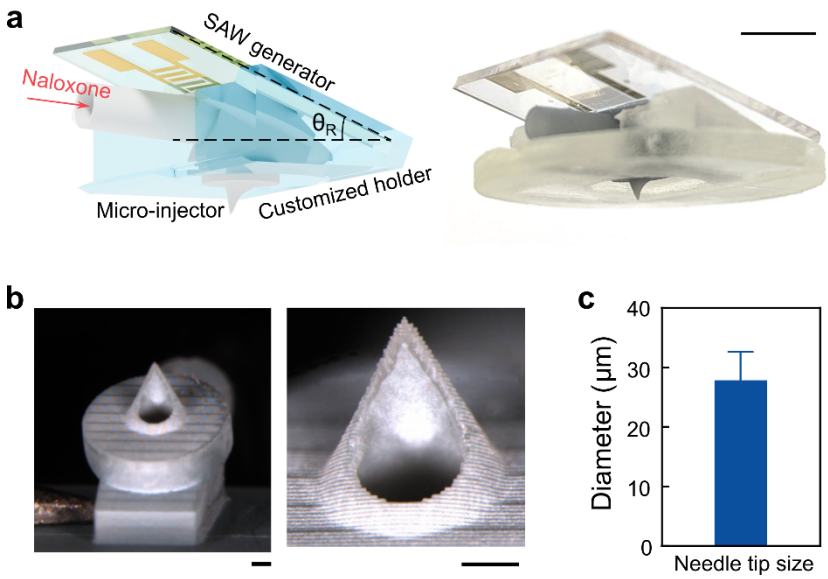

Supplementary Fig. 3 Design and fabrication of acoustofluidic patch devices. (**a**) Schematics and photos of the acoustofluidic delivery patch devices. (**b**) Photograph of the 3D printed microinjectors with sharp tips. (**c**) The corresponding measurement of the average tip diameter. (mean ± s.d., n = 4 independent devices, with three measurements per device).

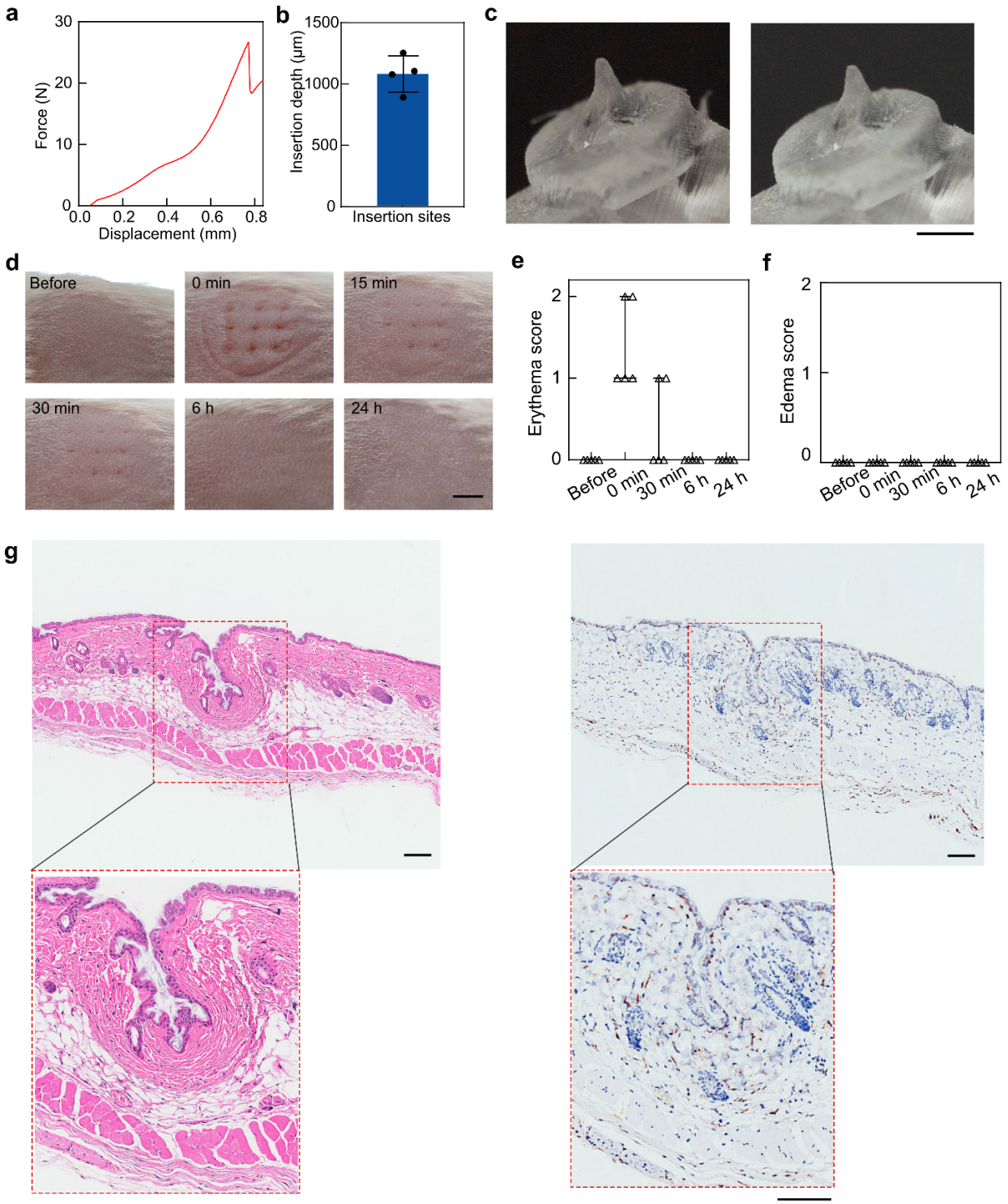

Supplementary Fig. 4 Minimally invasive insertion and skin compatibility. (**a**) Representative force–displacement curve during microneedle insertion, showing a clear penetration event characterized by a distinct force peak followed by a transient force drop, indicative of controlled insertion without excessive mechanical loading. Similar results were obtained from 3 independent devices. (**b**) Quantified insertion depth across multiple insertion sites (mean ± s.d., n = 4 independent devices), demonstrating consistent and shallow penetration compatible with minimally invasive delivery. (**c**) Optical images of the microneedle array before (left) and after

(right) insertion. Scale bar, 500 μm. Similar results were obtained from 3 independent devices. (**d**) In vivo skin recovery post acoustofluidic transdermal penetration. Time-lapse images show the mouse's skin recovery after the patch treatment. No visible irritation was observed 24 hours post patch application. Scale bar: 2 mm. Similar results were obtained from 3 independent mice. (**e**) Semi-quantitative erythema scores at indicated time points, revealing only transient and mild skin redness following insertion. n = 5 independent samples. (**f**) Edema scores over time, indicating negligible swelling throughout the observation period. n = 5 independent samples. (**g**) Representative H&E (left) and immunohistochemical staining for CD31/F4/80 (right) of skin sections collected 24 h after microneedle application following multiple system activations. Preserved skin architecture and only sparse immune cell presence are observed. Dashed red boxes indicate the insertion site. Scale bar, 100 μm. Similar results were obtained from 3 independent skin samples.

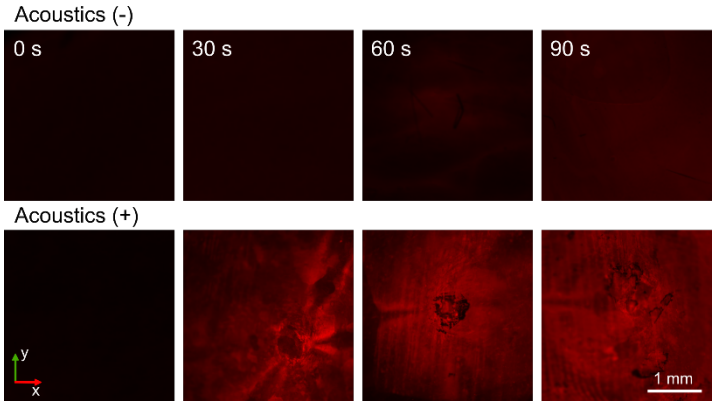

Supplementary Fig. 5 Acoustofluidic patch-mediated transdermal delivery ex vivo. The concentration in the stock solution of Rhodamine B is 10 mg/mL. Scale bars: 1 mm. Similar results were obtained from 3 independent experiments.

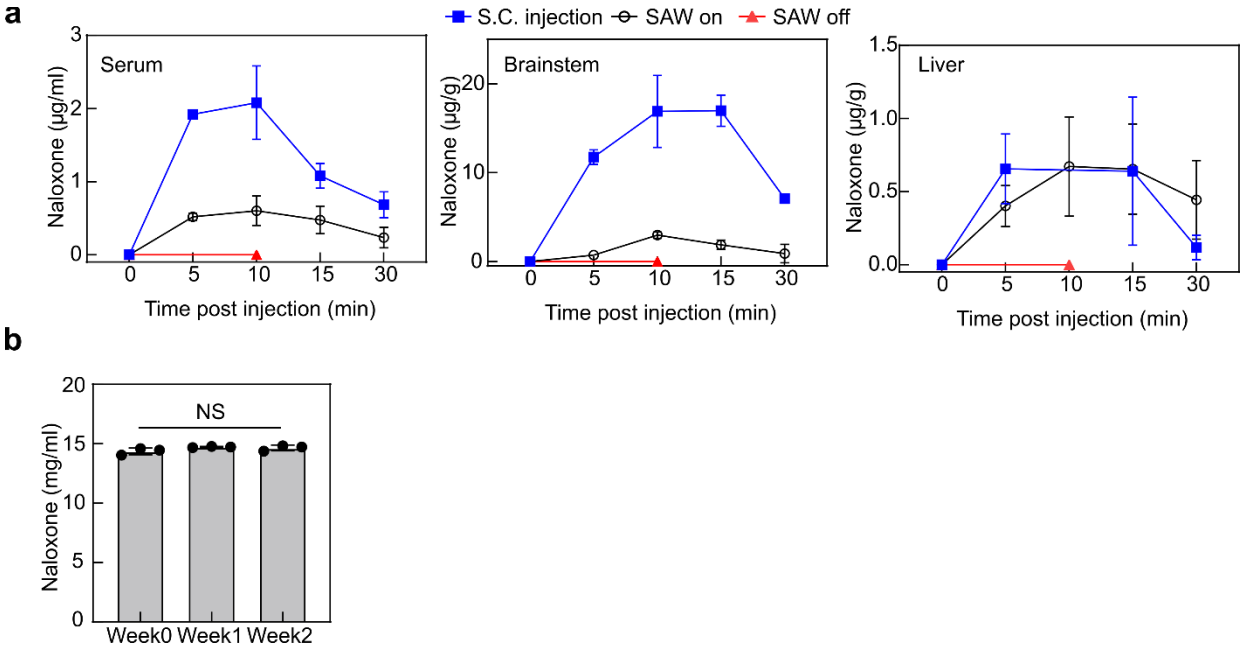

Supplementary Fig. 6 Biodistribution and pharmacokinetics of patch-mediated naloxone delivery. (**a**) Time-dependent naloxone concentrations measured in serum, brainstem, and liver following three delivery conditions: subcutaneous injection (blue), patch-based delivery with acoustic actuation (SAW on, black), and sham patch without acoustic actuation (SAW off, red). Concentrations were quantified by LC–MS/MS at indicated time points post-treatment. Naloxone levels under the sham patch condition remained at or near the detection limit across all tissues. Data are shown as mean ± s.d. (**b**) Stability of naloxone preparation delivered by the patch device over repeated use, assessed at Week 0, Week 1, and Week 2. No significant difference (NS) was observed across time points (one-way ANOVA). n = 3 independent experiments.

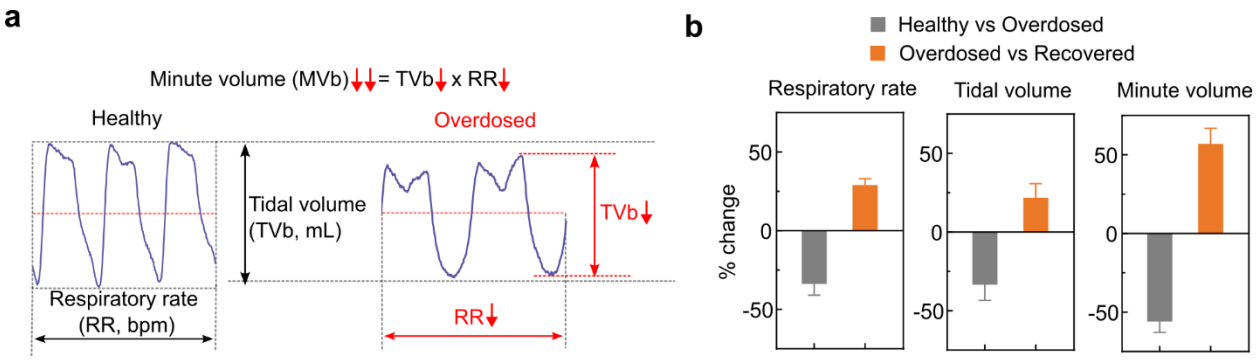

Supplementary Fig. 7 Measuring respiratory depression induced by opioid overdose. (**a**) Representative lung flow diagram showing the relationship between respiratory rate (RR), tidal volume (TVb), minute volume (MVb), and their corresponding change during overdose. (**b**) Percentage change comparison in the overdosed and recovered states, respectively (mean ± s.d., n = 10 independent mice). Minute volume is the product of the respiratory rate and tidal volume, showing the largest % decrease in the overdosed state as well as the largest % increase after recovery.

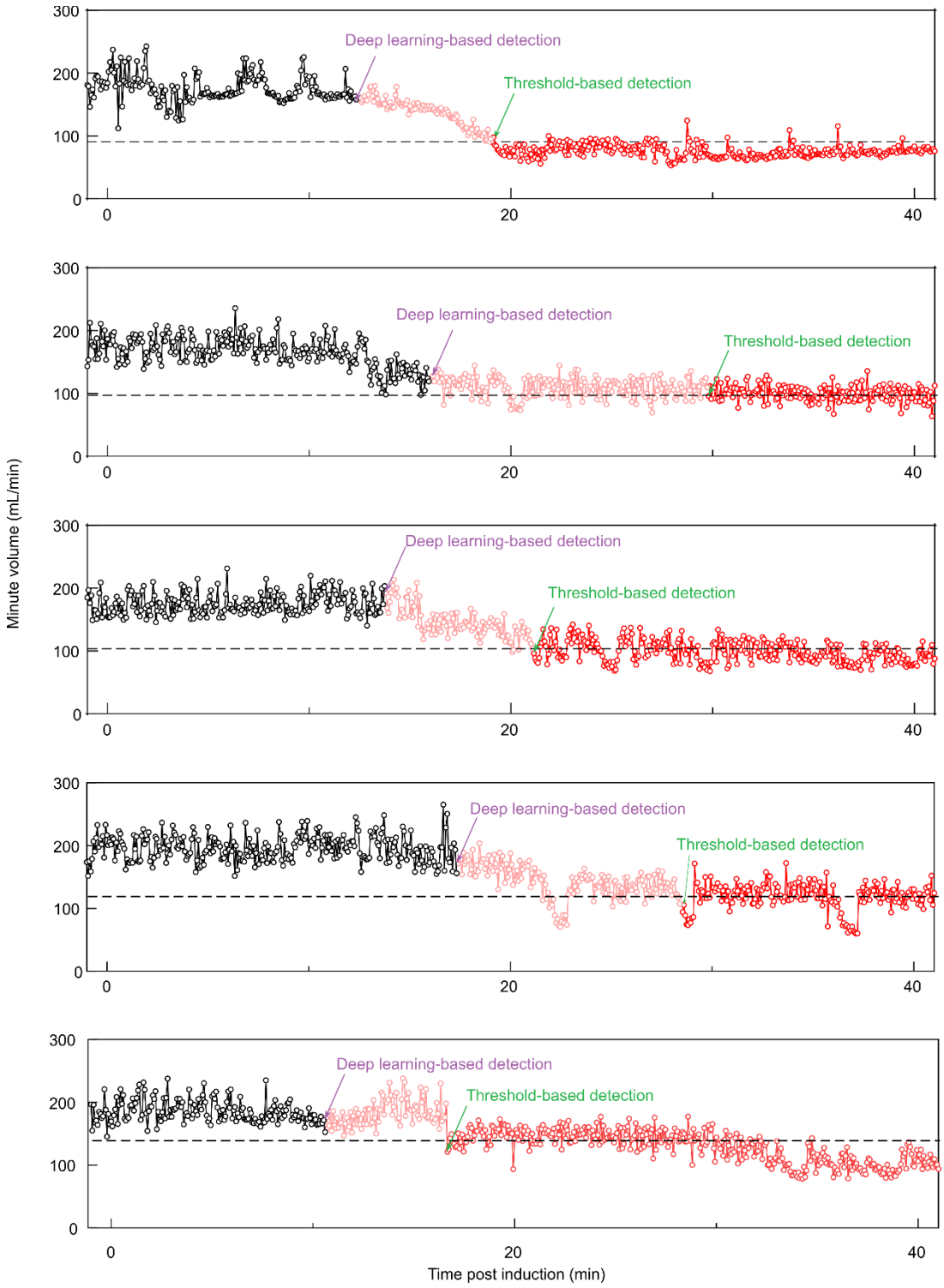

Supplementary Fig. 8 Comparison of deep learning-based detection and threshold-based detection in mice. The detected timepoints were labeled with light red for the deep learning-based method, and with dark red for the threshold-based method (over 50% decrease in ventilation).

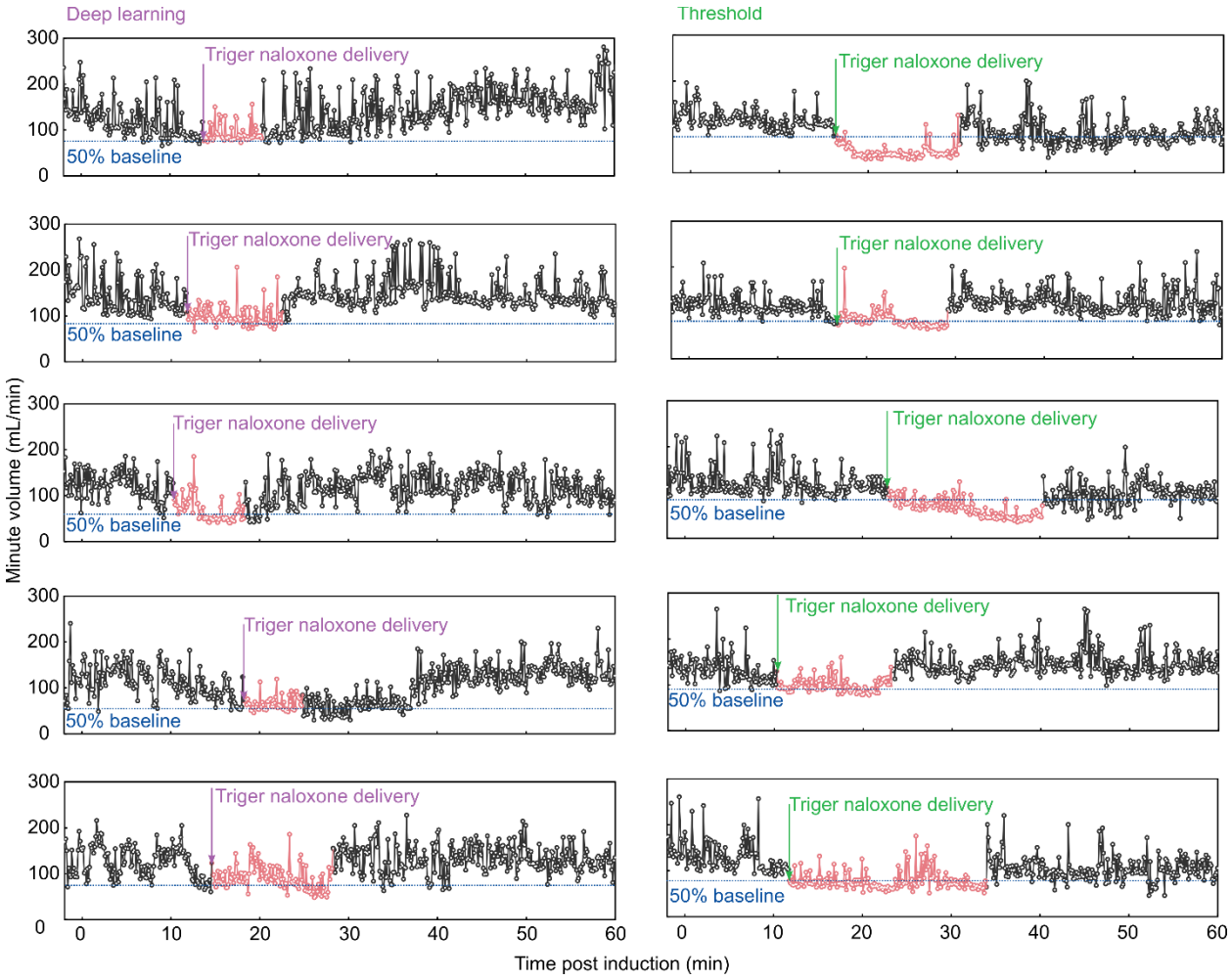

Supplementary Fig. 9 Comparison of intelligent-based (left column) and threshold-based (right column) closed-loop strategies in mice. The time points that the mouse was in the opioid overdose state are marked with red dots.

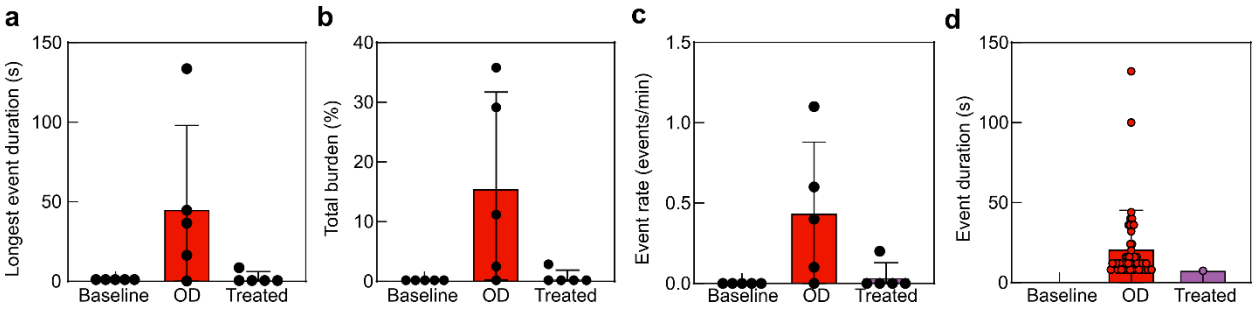

Supplementary Fig. 10 Respiratory suppression analysis after intelligent patch naloxone treatment. Respiratory suppression events were defined as continuous periods in which minute ventilation (MVb) remained below 50% of the mouse-specific healthy baseline for at least 8 s. Quantification of (a) longest event duration, (b) total suppression burden, and (c) event rate showed that fentanyl overdose markedly increased prolonged low-ventilation episodes, whereas patch-triggered naloxone treatment reduced these events to near-baseline levels. (d) Event duration distribution of all detected respiratory suppression events. Each dot represents one detected event. Baseline, healthy baseline period; OD, fentanyl overdose period; Treated, post-treatment recovery period. Data in a – c are presented as mean ± s.d. n = 5 independent mice.

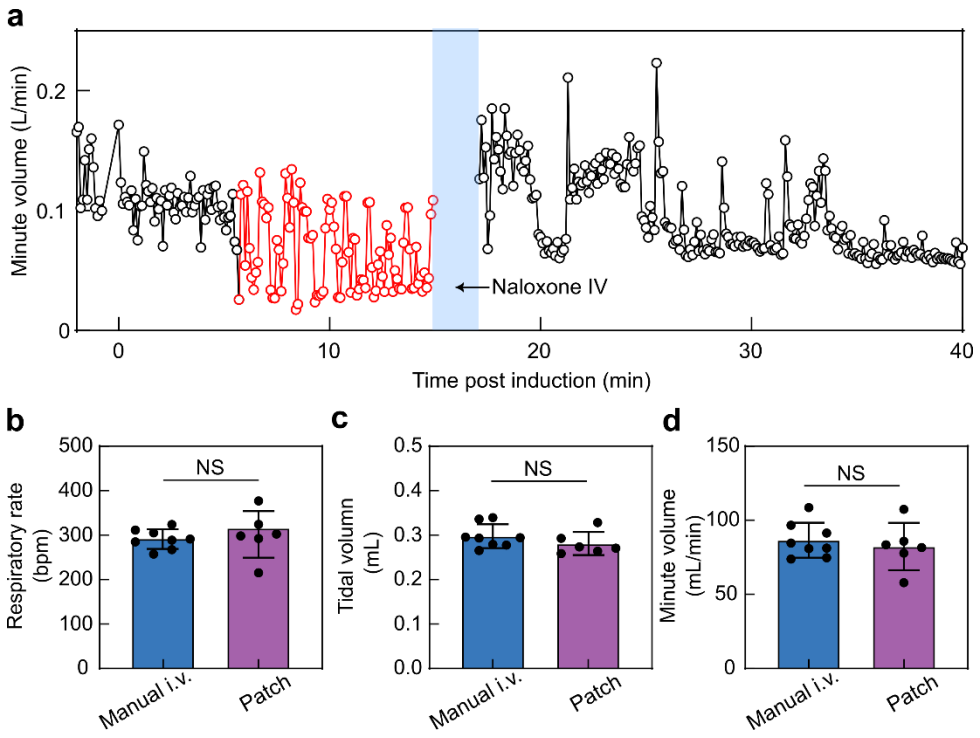

Supplementary Fig. 11 Comparison of intelligent patch treatment and manual i.v. administration. (**a**) Representative minute-volume trace showing fentanyl-induced respiratory depression followed by manual i.v. naloxone rescue at a matched intervention time. The red segment denotes the depressed respiratory state before naloxone rescue, and the blue shaded region marks the rescue window. (**b-d**) Respiratory recovery outcomes after rescue were comparable between manual i.v. naloxone and the closed-loop patch, as assessed by **b** respiratory rate, **c** tidal volume, and **d** minute volume. Data are shown as mean ± s.d.; n = 8 independent mice for the manual i.v. group and n = 6 independent mice for the patch group; NS, not significant.

Supplementary Table 1. Pharmacokinetic parameters of naloxone following patch-based delivery

Parameter	Serum (μg/mL), n = 4	Brainstem (μg/g), n = 3	Liver (μg/g), n = 3
Cmax (μg/mL)	1.162 (0.963–1.362)	4.449 (3.736–5.325)	1.617 (1.280–2.014)
tmax (min)	10.0 (6.25–13.75)	11.67 (10.0–15.0)	10.0 (5.0–15.0)
AUC0–30 (μg·min/mL)	20.18 (17.26–22.04)	72.72 (48.82–88.04)	31.56 (27.43–34.66)